Published in final edited form as:
Magn Reson Med. 2010 April ; 63(4): 959–969. doi:10.1002/mrm.22222.

Improvements in Parallel Imaging Accelerated Functional MRI Using Multiecho Echo-Planar Imaging

Heiko Schmiedeskamp[1,2], **Rexford D. Newbould**[1,3], **Laura J. Pisani**[1], **Stefan Skare**[1], **Gary H. Glover**[1], **Klaas P. Pruessmann**[2], and **Roland Bammer**[1,*]

[1]Lucas Center, Department of Radiology, Stanford University, Stanford, California, USA [2]Institute for Biomedical Engineering, University and ETH Zurich, Zurich, Switzerland [3]GSK Clinical Imaging Centre, London, United Kingdom

Abstract

Multiecho echo-planar imaging (EPI) was implemented for blood-oxygenation-level-dependent functional MRI at 1.5 T and compared to single-echo EPI with and without parallel imaging acceleration. A time-normalized breath-hold task using a block design functional MRI protocol was carried out in combination with up to four echo trains per excitation and parallel imaging acceleration factors $R = 1–3$. Experiments were conducted in five human subjects, each scanned in three sessions. Across all reduction factors, both signal-to-fluctuation-noise ratio and the total number of activated voxels were significantly lower using a single-echo EPI pulse sequence compared with the multiecho approach. Signal-to-fluctuation-noise ratio and total number of activated voxels were also considerably reduced for nonaccelerated conventional single-echo EPI when compared to three-echo measurements with $R = 2$. Parallel imaging accelerated multiecho EPI reduced geometric distortions and signal dropout, while it increased blood-oxygenation-level-dependent signal sensitivity all over the brain, particularly in regions with short underlying T_2^*. Thus, the presented method showed multiple advantages over conventional single-echo EPI for standard blood-oxygenation-level-dependent functional MRI experiments.

Keywords

fMRI; parallel imaging; multiecho EPI; temporal SNR; image distortions; signal dropout

Single-shot gradient echo echo-planar imaging (EPI) is currently the most commonly used pulse sequence for functional MRI (fMRI) because of its robustness and rapid image formation capability. However, there are considerable issues in image quality associated with this sequence (1). Specifically, geometric distortions from off-resonant spins, image blurring, and substantial signal dropout in regions affected by large susceptibility gradients are major issues. Parallel imaging has been suggested to reduce these problems (2,3) by increasing the bandwidth per pixel along the phase-encoding direction, thus shortening the EPI readout train.

*Correspondence to: Roland Bammer, Ph.D., Stanford University, Department of Radiology, Lucas Center, 1201 Welch Road, Stanford, CA 94305-5488. rbammer@stanford.edu.

Presented in part at the Joint Annual Meeting of the ISMRM-ESMRMB, Berlin, Germany, 2007.

The use of parallel imaging allows one to acquire images with at least the same temporal resolution as for single-shot EPI, with the added benefit of reducing image artifacts to a level usually only achieved with interleaved EPI acquisitions. Interleaved EPI, in turn, can be affected by motion artifacts, which may add unwanted fluctuations to the fMRI signal. Moreover, interleaved EPI cannot provide high temporal resolution because *k*-space data from several interleaves need to be combined to form a fully sampled *k*-space.

A shortened EPI train—enabled by parallel imaging—affords the inclusion of additional EPI trains (echoes) between radiofrequency excitation and the usual image formation in fMRI at a late echo time (TE) (e.g., 50 ms at 1.5 T), as well as between this late echo and the excitation of the subsequent slice. Thus, it can be assumed that a longer total acquisition duration could increase the overall signal-to-noise ratio (SNR) and compensate for the SNR loss induced by the utilization of parallel imaging (4).

Recently, a multiecho, multishot, parallel imaging EPI sequence named PERMEATE (perfusion with multiple echoes and temporal enhancement) has demonstrated multiple advantages over single-echo single-shot EPI for perfusion-weighted MRI (5,6). Since both perfusion-weighted MRI and blood-oxygenation-level-dependent (BOLD)-fMRI (7,8) depend inherently on T_2^*-related signal attenuation, parallel imaging accelerated multiecho EPI might be of equal benefit for fMRI.

A single-shot multiecho EPI acquisition technique with high temporal resolution suitable for fMRI was introduced by Speck and Hennig (9). They measured T_2^* and S_0 (the signal strength at the time of radiofrequency excitation) and performed per-voxel BOLD-fMRI analysis on relative changes of these values. Posse et al. (10) presented a proton echoplanar spectroscopic imaging sequence for multiecho signal acquisition and combined all echo images of a given excitation to form a composite image for subsequent fMRI analysis. Their study was the first to demonstrate enhanced BOLD-contrast with multi-echo EPI when compared to single-echo EPI methods, however limited by a reduced maximum number of slices or an increase in pulse repetition time (TR). This method was later used to improve BOLD-signal detection in real-time fMRI (11), as well as to study global changes in brain perfusion upon graded hypo- and hypercapnia (12). The latter took advantage of the T_2^*- and S_0-mapping capabilities of multiecho EPI techniques. Furthermore, the availability of multiple echo images allows the inclusion of additional compensation gradients preceding the readout of individual echo images, facilitating susceptibility-compensated acquisitions evaluated using a hypercapnic challenge (13). Multiecho EPI was also applied toward image distortion correction for real-time fMRI by alternating the polarity of the phase-encoding gradients during the acquisition of the second echo image (14). Poser et al. (15) showed that multiecho EPI with parallel imaging could enhance BOLD-sensitivity compared to single-echo EPI. Their measurements demonstrated improvements in expected BOLD contrast-to-noise ratio at 3 T, retrieved from stimulation-free resting-state acquisitions. Unfortunately, they could not draw quantitative conclusions from functional data using a Stroop interference task (16) due to large variations in functional activity among subjects.

The purpose of the present study was to determine the benefits of adding multiple echoes and parallel imaging to single-shot EPI under minimization of intersubject variations in functional activity and with the condition of unchanged TR. We used a breath-hold paradigm to induce BOLD-signal changes in the entire brain. For all experiments using different parallel imaging reduction factors, TR and the total acquisition duration were kept constant. We examined whether or not higher BOLD-sensitivity could be achieved with a multiecho approach compared with conventional single-echo, single-shot, gradient echo EPI. Furthermore, the effect of this approach on signal-to-fluctuation-noise ratio (SFNR),

i.e., temporal SNR, a measure for the amount of detectable functional activity incorporating physiologic noise (17), was explored.

Overall, we aimed at quantifying BOLD-contrast enhancement with unchanged TR and acquisition time, which limits the maximum number of echo images and thus the achievable sensitivity gain. However, our method is suitable for whole-brain fMRI analysis without additional time penalty typically induced by other multiecho acquisition techniques. Therefore, our pulse sequence can be used as an alternative to standard EPI sequences for whole-brain fMRI with the same timing parameters.

MATERIALS AND METHODS

MR Image Acquisition

A multiecho multishot gradient echo EPI sequence, PERMEATE (5), was implemented for fMRI data acquisition on a 1.5 T GE Signa 12.0 Excite whole-body scanner (GE Healthcare, Waukesha, WI), with maximum gradient strength = 50 mT/m and slew rate = 150 T/m/sec. An eight-channel phased-array head receiver coil (InVivo Corporation, Orlando, FL) was used for signal reception; the quadrature body resonator, for radiofrequency excitation. The PERMEATE pulse sequence commences with a water-selective spectral-spatial excitation pulse to reduce chemical shift artifacts from lipids. The excitation pulse is then followed by a series of M short EPI trains to enable a multiecho readout at TE ranging from TE_1 to TE_M (Fig. 1). Using parallel imaging, multiple echo images can be acquired within the same time window required for a nonaccelerated single-echo measurement, since the acquisition time for one EPI echo train is significantly shorter (shortened by factor R) compared to nonaccelerated acquisitions. Therefore, the use of parallel imaging facilitates the acquisition of multiple echoes while maintaining total acquisition time.

- The following acquisition parameters were set for the fMRI experiments: matrix size = 80 × 80 (78 × 78 in case of acquisitions with a parallel imaging reduction factor R = 3), number of slices = 24, slice thickness = 3mm (1mm skip between adjacent slices), field of view = 24 cm, isotropic voxel size = $3mm^3$, TR = 2 sec, flip angle = 80° (approximately equal to the Ernst angle for gray matter), number of volumes per fMRI experiment = 157.

The first four volumes of each experiment were discarded to avoid nonequilibrium effects; after that, a steady-state signal was assumed. M echo trains followed each other immediately. Parallel imaging reduction factors R ranged from 1 (no parallel imaging acceleration) to 3 (3-fold acceleration), resulting in EPI echo train lengths according to Table 1. The EPI echo train length in an acquisition with given R and acquisition matrix size determined the maximum number of echo trains per TR, given a previously fixed number of slices.

Common methods for calculations of optimal contrast for BOLD-fMRI experiments result in TE ≈ T_2^* (10,18). At 1.5 T, T_2^* in homogeneous brain regions is in the range of 60–70 ms; however, near-optimal BOLD-sensitivity can be reached with a wider range of TE between 50 and 80 ms (19). Recently, a new model for optimal BOLD-contrast—accounting for heterogeneous sources of noise—was presented, predicting that the extent of BOLD-signal changes varies only slowly with TE (20). With these factors in mind, we assumed that there are no tight boundaries for optimal TE. For measurements with R = 1 and R = 3, we acquired one of the echo images at TE = 50 ms; in case of R = 2, the “optimal” echo image was obtained at TE = 61.1 ms. Data measured at these TE were used for single-echo comparisons of fMRI experiments acquired with different reduction factors. For each R, additional TE to acquire multiecho data were chosen according to Table 1, with TR and the number of slices

kept constant in all scans. Thus, single-echo data vs multiecho data for each *R* were compared based on the same dataset to avoid interscan variability.

Image Reconstruction

Parallel imaging reconstruction was performed using GRAPPA (Generalized autocalibrating partially parallel acquisitions) calibration with a two-dimensional kernel size of 2 × 5 *k*-space points (21,22). The first *R* acquisitions of each fMRI time series were obtained as interleaved EPI scans to reconstruct a fully sampled image. This combined image served as a calibration set for the determination of the GRAPPA weights. Once enough interleaves were acquired to determine the GRAPPA weights, interleaved acquisition was discontinued. Only the first interleave containing *R*-fold accelerated echo trains was repeated for subsequent time points. From each of these *R*-fold undersampled *k*-space trajectories and for each of the *M* echoes, images were reconstructed separately using the estimated GRAPPA weights, so temporal resolution of each fMRI experiment was equal to one TR of the sequence.

fMRI Experiments

Breath-hold experiments were conducted to evaluate signal stability (SNR and SFNR) and the extent of BOLD-signal changes detected with the PERMEATE sequence using different *R*s and *M*s. Breath holding and other forms of hypercapnia, unlike sensory-motor stimuli, affect the BOLD signal in gray matter within the entire brain by altering local cerebral blood oxygenation (23). The advantages of breath-hold tasks over sensory-motor stimuli are their independence of cognitive control over stimulus and response. Reproducibility of fMRI data is a major concern in comparative evaluations with different pulse sequences or with varying parameters. To keep the BOLD-signal response as constant as possible, the respiration of each volunteer was monitored by a respiration sensor. An experiment was stopped if the respiration was irregular or the volunteer was not following the instructions for each breath-hold period. Besides better reproducibility, another reason for choosing a breath-hold experiment for our analysis was that both regions affected by signal dropout (short T_2^*) and homogeneous brain regions showed detectable BOLD-signal changes, giving more information about the efficacy of the multi-echo acquisition. A similar breath-hold task has been used successfully for calibration purposes (24) in multisite fMRI studies in the Function Biomedical Informatics Research Network project (NIH-NCRR, Bethesda, MD).

Five healthy volunteers were recruited for three sessions each, after they gave informed consent according to a protocol approved by the institutional review board. In every session, the volunteers performed four breath-hold experiments. The purpose of the first run was to "warm up" the scanner, as well as to accustom the volunteer to the scan and a constant level of inspiration (practice session). The subsequent sessions consisted of measurements with three different reduction factors, ranging from 1 to 3, in alternating order to counterbalance possible habituation effects. The volunteers were asked to breathe regularly for 16.5 sec (baseline), breathe in for 3 sec, and hold their breaths for another 16.5 sec (deactivation). This cycle was repeated eight times, finishing with an additional period of regular respiration. In these experiments, the total acquisition time for each fMRI dataset was 5 min 6 sec, excluding prescan and discarded acquisitions before a steady-state signal was reached.

All acquisitions were triggered with the presentation of the paradigm prompts to the subject to obtain a synchronous timing of the stimulus with the measurements. The paradigms were controlled and presented to the subject, using a commercial software product (E-Prime; Psychology Software Tools, Pittsburgh, PA).

Data Preprocessing

After image reconstruction, individual volumes acquired at intervals of TR were corrected for rigid-body motion using SPM5 (Wellcome Department of Imaging Neuroscience, UCL, London, United Kingdom).

Thereafter, the individual echoes for each time point were combined in two different ways for fMRI analysis. First, all *M* echoes observed at a given time point were combined by simple echo summation to form a new composite image (10,15,25). This method is henceforth called *echo summation*. Alternatively, the images observed at different TEs were weighted on a per-voxel basis by the calculated underlying T_2^* (10,15). This approach is referred to as T_2^**-weighted echo combination*. The T_2^* map was estimated by fitting an exponential decay using a signal-intensity-weighted least-squares fit for all echoes of a given acquisition.

Using the estimated T_2^*, echo weighting was performed for every voxel within the brain with a signal intensity above a specified threshold. For T_2^*-weighted echo combination, the individual echo images were summed using

$$S_{weighted} = \sum_{m=1}^{M} W(TE_m) \cdot S_{m,data}, \quad [1]$$

where

$$w(TE_m) = TE_m \cdot e^{-TE_m \cdot R_{2fit}^*}. \quad [2]$$

Here, $S_{\mathrm{m,data}}$ stands for the signal acquired at $\mathrm{TE_m} \cdot R_{2fit}^* = 1/T_{2fit}^*$ was extracted from the aforementioned T_2^* map. Posse et al. (10) described this weighting function in more detail. Equation 1 weights the individual echo images of an acquisition such that the echo image with TE closest to the underlying tissue T_2^* is emphasized most, that is, it contributes to the largest extent in the total weighted signal. In other words, for voxels with a short underlying T_2^*, more emphasis is put on echo images with a short TE, while for voxels with a higher T_2^* the echo images with longer TE are more heavily weighted. In principle, the time course of the fitted T_2^* could be used for fMRI analysis (9). However, as T_2^* decays exponentially, the dynamic range (relative to the noise level) would be much smaller. Thus, BOLD-signal analysis of the T_2^* time course alone would yield less sensitivity than the analysis of the weighted echo images.

As a final preprocessing step, linear drifts in the time series were eliminated for each voxel prior to fMRI analysis.

fMRI Analysis

The correlation between the fMRI time series and both a sine wave (r_{sin}) and a cosine wave (r_{cos}) was determined using Pearson's correlation coefficient on a voxel-by-voxel basis. The final correlation coefficient *r* used for fMRI analysis was the root-sum-of-squares combination of both coefficients, as described by Lee et al. (26):

$$r = \sqrt{r_{\sin}^2 + r_{\cos}^2}. \quad [3]$$

An advantage of this procedure is that it does not require an accurate choice of the delay in the hemodynamic response function (27) for a given subject.

Every voxel within the brain with a correlation coefficient r of 0.3 or higher was deemed activated by the functional task.

SNR and SFNR Calculations

Regional SNR was calculated from two consecutive images within the fMRI time series (S_A and S_B), using the difference method (28,29):

$$SNR|_{ROI} = \frac{mean\,(S_A + S_B)|_{ROI}}{\sqrt{2} \cdot std\,(S_A - S_B)|_{ROI}}. \quad [4]$$

Here, the average signal from the sum of two images in the selected region of interest was divided by the standard deviation of the difference of the same consecutive images in the same region of interest. SNR was extracted from a spherical region of interest in the center of the brain, where SNR is minimal due to the physical distance to the coil elements and the use of parallel imaging. It contained approximately 2% of all acquired voxels. SNR was calculated for every two consecutive images within the entire fMRI time series, resulting in $n - 1$ SNR values for an fMRI experiment with n time points. The SNR reported in this study was the average of the $n - 1$ SNR values. A similar approach was used by Glover and Lai (30).

SFNR was calculated for each voxel separately by dividing the average signal over time by its standard deviation:

$$SFNR = \frac{\frac{1}{n} \cdot \sum_{t=1}^{n} S\,(t)}{\sigma_t} \quad [5]$$

Here, σ_t is the standard deviation over time for a particular voxel with an observed signal $S(t)$. SFNR was averaged over the entire brain to obtain a single value for each subject and session. Furthermore, voxel-wise SFNR maps were produced.

High SFNR is expected to be more important for fMRI than raw SNR as the relative change in signal over time is the critical factor for correlation analysis and other statistical calculations for fMRI time series, and SFNR contains information about physiologic noise. Hence, high fluctuation due to bulk motion or spatial-temporal *noise* variation should be minimized. In fMRI acquisitions using parallel imaging, SFNR loss depends on the noise ratio between parallel imaging accelerated (σ_{red}) and nonaccelerated (σ_{full}) image acquisition (31):

$$\frac{\sigma_{red}^2}{\sigma_{full}^2} = 1 + \frac{\sigma_{I,full}^2}{\sigma_{full}^2} \cdot \left(g^2 \cdot R - 1\right). \quad [6]$$

Here, the geometry factor g expresses the parallel imaging–induced spatially varying noise. The *g*-factor depends on the geometrical arrangement of the coil elements and the parallel imaging reduction factor *R*. Physiologic noise depends on the MR signal strength, TE and ΔT_2^* (BOLD-signal induced change in T_2^*), but does not change with a change in *R* or g. In the case of a total dominance of image noise (σ_I) (i.e., system imperfections in the gradients, radiofrequency pulses, and shim coils) the temporal signal variance is amplified by $g^2 \cdot R$. However, if physiologic noise dominates the fMRI time series, σ_{red} would approach σ_{full}, i.e., parallel imaging would not influence the SFNR of the fMRI experiment. According to Poser et al. (15) and de Zwart et al. (31), the relative amount of physiological noise to total noise determines the drawback in temporal signal stability for parallel imaging accelerated measurements. This is of particular relevance for high-field imaging as the physiologic noise component increases (17) while the *g*-factor noise enhancement decreases (32).

All calculations used in the present study were implemented in MATLAB 7 (The MathWorks, Natick, MA).

RESULTS

Analsis of Echo Combination Schemes vs Single-Echo Data

SFNR maps processed using the aforementioned echo combination schemes (echo summation or T_2^*-weighted echo combination) were compared to SFNR maps of the individual echo images. Figure 2 presents SFNR maps for acquisitions with reduction factors *R* = 1–3, obtained from session 3 of subject #1. Similar maps were produced for all other volunteers and sessions (images not shown). Due to the T_2^*-decay of the signal, SFNR decreased exponentially as TE increased. Figure 3 shows the mean SFNR averaged over all subjects and sessions as a function of TE and *R* and compares these values to a monoexponential decay with $\exp\left(-\mathrm{TE}/\mathrm{T}_2^*\right)$, for a uniform T_2^*=65ms.

The measured SFNR values closely followed the predicted decay (dotted lines in Fig. 3); thus, the smaller the TE, the larger the SFNR. Moreover, T_2^*-related signal dropout due to susceptibility gradients near air-tissue interfaces was much less apparent on echo images obtained with shorter TE (cf. Fig. 2). However, in acquisitions with *R* = 2 and *R* = 3, for images with the shortest TE compared to those with longer TE the total number of activated voxels (TNAV) was considerably lower in homogeneous brain regions (cf. Table 2, Fig. 4). Echo images with shorter TE and those with longer TE both have their particular advantages for fMRI, depending on the brain region of interest. Thus, the combination of multiple echo images takes advantage of higher BOLD contrast at longer TE and less signal dropout in images acquired at shorter TE.

Both echo combination schemes clearly demonstrated superior SFNR and SNR when compared to any single-echo image of the same acquisition (see Table 2). Measurements with *R* = 2 resulted in overall average SFNR (SNR) of 92.5 ± 6.0 (77.3 ± 6.2) for echo summation, and 86.8 ± 5.5 (74.8 ± 4.5) for T_2^*-weighted echo combination, while analysis of individual echo images gave rise to values of 80.2 ± 4.4 (63.5 ± 3.8) for the first echo, 58.7 ± 3.1 (48.3 ± 2.6) for the second echo, and 44.0 ± 2.3 (37.1 ± 1.9) for the third echo. Similar results obtained from acquisitions with *R* = 3 are presented in Table 2. Furthermore, for multiecho vs single-echo acquisitions acquired at TE > 40 ms, not only was SFNR higher but also signal dropout was reduced. Echo summation yielded slightly higher SFNR values than T_2^*-weighted echo combination because echo summation added all echo images without weighting; therefore, the relative contribution from the first echo image was bigger for regions with long T_2^*.

Figure 4 represents fMRI maps of acquisitions with R = 1–3, corresponding to the SFNR maps in Fig. 2. TNAV for R = 2 and R = 3 was much higher for both echo combination schemes compared to any single-echo image of the same acquisition. This was the case for the experiment shown in Figs. 2 and 4 and for all other volunteers (see Table 2). These results underline the added benefit of a multiecho approach. On average over all volunteers and sessions, TNAV of echo summation (T_2^*-weighted echo combination) was 55% (57%) higher compared to TNAV of the single-echo image with the highest BOLD-contrast when R = 2 was applied. The corresponding increase for measurements with R = 3 was 92% (94%). Thus, not only SFNR but also TNAV increased upon combination of multiple echoes. There was no significant difference in the BOLD-fMRI signal between the two echo combination schemes. In homogeneous brain regions, the difference between echo summation and T_2^*-weighted echo combination was small, i.e., the weights applied to the individual voxels were almost the same. In case of R = 2, the normalized weights produced with T_2^*-weighted echo combination for a voxel with T_2^*=65 ms in echo images 1 to 3 were 0.25, 0.36, and 0.39 compared to equal weighting of 0.33 in case echo summation was applied. Functional activity was mainly detected in homogeneous brain regions, providing an explanation for similar results from the two echo combination schemes.

Comparison of Single-Echo EPI Acquisitions With Different Reduction Factors *R*

For an echo image at TE = 50 ms, the average SFNR values over all subjects and sessions in measurements with R = 1, 2, and 3 were 66.7, 51.4 (this particular value was estimated from the fitted data in Fig. 3), and 39.1, respectively. These numbers are equivalent to an overall loss in SFNR of 22.8% for R = 2 and a loss of 41.4% for R = 3. Similar results were obtained in SNR measurements. Thus, SNR and SFNR dropped with increasing reduction factor. This is due to the $\left(g \cdot \sqrt{R}\right)$ – fold S(F)NR penalty for a shorter readout in parallel imaging, when physiologic sources do not dominate the total noise. The use of parallel imaging has considerable consequences for fMRI experiments since lower SFNR, while TE is kept constant, decreases the sensitivity to changes in the BOLD signal. The resulting average TNAV over all subjects was therefore 31% higher for measurements with R = 1 and M = 1 compared to the analysis of any single echo acquisition with R = 2. Compared to R = 3, the increase in TNAV was even more pronounced (+106%). Even though parallel imaging might reduce geometric distortions, such a difference in BOLD sensitivity would mostly prevent single-echo measurements with parallel imaging from being applied to fMRI, particularly at 1.5 T, where physiological noise is small compared to other noise sources.

Multiecho EPI With *R* = 2 and *R* = 3 vs Nonaccelerated Single-Echo EPI

In contrast, the combination of multiple echo images compensated for the parallel imaging-induced loss in SFNR, SNR, and TNAV compared to conventional single-shot single-echo (R = 1, M = 1) EPI acquisitions. The average SFNR (SNR) over all subjects and sessions for echo summation was 39% (35%) higher for R = 2, M = 3, and 14% (12%) higher for R = 3, M =4. For T_2^*-weighted echo combination, average SFNR (SNR) increased by 30% (31%) for R = 2, M = 3, and 9% (10%) for R = 3, M = 4. SFNR maps in Fig. 2 not only revealed higher SFNR for parallel imaging-accelerated multiecho acquisitions (Fig. 2e,f with R = 2 and Fig. 2k,l with R = 3 vs Fig. 2a with R = 1) but also considerably reduced image blurring and signal dropout.

TNAV was measured with the threshold r = 0.3. From the fMRI analysis of the breath-hold data (see Fig. 4), PERMEATE with R = 2 and M = 3(T_2^*-weighted echo summation) showed the highest level of detected changes of the BOLD signal averaged over all subjects and sessions (TNAV = 13,855 ± 1318). Compared to conventional single-shot EPI (TNAV =

11,594 ± 2182), we saw an average increase in TNAV of 19%. For PERMEATE with $R = 3$ and $M = 4$, TNAV was reduced by 6% (TNAV = 10,913 ± 3043).

Region-Specific Analysis of Multiecho EPI With $R = 2$ and $R = 3$ vs Single-Echo EPI With $R = 1$

Region-specific analysis of fMRI activity revealed additional detail about the benefits of multiecho acquisitions. In addition to higher overall TNAV, the extent of signal dropout was remarkably reduced in acquisitions with reduction factors of 2 or 3. It was therefore possible to measure additional BOLD-signal changes using PERMEATE with $R = 2$ or $R = 3$ in areas typically prone to signal dropout. Figure 5 presents two slices of the same volunteer shown in Fig. 2, taken from the lower part of the brain where strong signal dropout occurred close to the ear canals and nasal cavities. T_2^* was very short in such regions (cf. T_2^*-map in Fig. 5d, calculated from exponential fitting of individual echo images); therefore, most of the signal dephased prior to the actual readout of the nonaccelerated acquisitions at TE = 50 ms. However, readouts with short TE in acquisitions with $R = 2$ and $R = 3$ detected BOLD-signal changes in signal dropout areas.

We divided the whole brain into three separate regions: a first region comprising voxels with low SFNR, a second region with voxels of average SFNR, and a third region including voxels with high SFNR (cf. Fig. 6a). These regions were then analyzed separately for acquisitions with (1) $R = 1$, $M = 1$, (2) $R = 2$, $M = 3$, (3) $R = 3$, $M = 4$. For this comparison, we analyzed multiecho data produced with T_2^*-weighted echo combination. Measurements with $R = 2$ outperformed the other two acquisition schemes in all three regions, averaged over all subjects and sessions (see Fig. 6b). For regions 1 to 3, average TNAV for multiecho measurements with $R = 2$ (given the correlation coefficient threshold $r = 0.3$) was 3%, 14%, and 21% higher compared with single-echo acquisitions using $R = 1$. For measurement using $R = 3$, TNAV decreased by 16% for region 1 and 13% for region 2 and increased by 7% for region 3. Given $r = 0.3$, parallel imaging accelerated multiecho EPI acquisitions with $R = 2$ provided particular advantages in regions with average to high SFNR, while the results in regions with lower SFNR were slightly higher compared with the standard acquisition scheme. For $R = 3$, TNAV decreased for regions with average to low SFNR, while an increase in TNAV was seen in regions with high underlying SFNR. Figure 6c shows distributions of correlation coefficients retrieved from all subjects and sessions as a function of specific region and acquisition scheme. This figure shows that multiecho acquisitions added additional statistical power, particularly to voxels with a very high correlation coefficient; in all three regions given a threshold of $r \approx 0.6$, multiecho acquisitions with $R = 2$ and $R = 3$ outperformed formed single-echo EPI acquisitions with $R = 1$.

DISCUSSION

Independent of the subject or the parallel imaging reduction factor used in this study, we found that both the temporal signal stability and the level of detected BOLD-signal changes increased when multiple echo images were combined compared to single-echo images (TE > 40 ms) measured with the same reduction factor. It is therefore preferable to use a multiecho approach as long as the readout duration for a single EPI echo train is short enough to facilitate the inclusion of additional EPI readouts prior to a TE that is deemed optimal for fMRI. For an acquisition matrix size of 80 × 80 voxels, this is the case for $R \geq 2$. Moreover, the multiecho approach using parallel imaging performed well compared to conventional nonaccelerated single-echo EPI measurements in areas not affected by large susceptibility effects. For regions with substantially shorter T_2^*, such as in the frontal lobe near the sinuses, considerably larger SFNR, together with an enhancement in BOLD sensitivity, was found with the parallel imaging accelerated multiecho EPI sequence presented.

Region-specific analysis revealed that our multiecho EPI approach was particularly suitable for regions with high underlying SFNR. In regions with low SFNR (excluding mere dropout regions), the enhanced *g*-factor noise in parallel imaging accelerated acquisitions offset the benefit of signal contributions from the additional echo images. In these regions, we saw a small increase in TNAV using acquisitions with $R = 2$ and $M = 3$ compared to standard acquisitions.

Intuitively, improved detection of BOLD-signal changes in the multiecho approach could be explained by the acquisition of additional echo trains. As SNR is proportional to the square root of the total sampling time, the addition of *M* echo trains would increase image SNR by the square root of *M* if there were no exponential signal decay, counteracting the parallel imaging–induced $\left(g \cdot \sqrt{R}\right)$-fold loss in SNR (4). Therefore, it makes sense to incorporate additional echo trains in parallel imaging–accelerated fMRI pulse sequences instead of to wait for the readout of a single echo train at TE. In addition, with the readout of multiple echo trains the center of *k*-space is sampled $M - 1$ times more often. However, things are more complex as BOLD contrast-to-noise ratio varies with TE and T_2^*. Certainly, a great advantage of the multiecho approach results from the fact that some of the signal from regions with a substantial susceptibility gradient is restored by the acquisition of data at shorter TE. In regions of shorter T_2^*, the optimal fMRI sensitivity is pushed toward shorter TE. The acquisition of multiple echo trains facilitates adequate BOLD-signal detection (i.e., multiecho acquisition lifts more voxels above the SNR required for adequate activation detection) for different brain areas with varying underlying T_2^*, including regions that are otherwise prone to signal dropout. Such regions adjacent to nasal cavities, auditory canals, and other air-tissue interfaces host important areas of the brain. Among them, for example, are the prefrontal cortex, the hippocampus, the posterior fossa, and the olfactory cortex.

On average over all subjects and sessions, the T_2^*-weighted echo combination gave rise to a slightly higher TNAV than mere echo summation. These findings are in agreement with Poser et al. (15). The T_2^*-weighting scheme has the advantage that it allows a high BOLD sensitivity over a larger range of underlying T_2^*. In regions with large signal dropout due to intravoxel dephasing, the signal from later echo images had most likely vanished. Using this weighting scheme, the composite signal in areas with large dropout was almost entirely determined by the earliest echo. In such cases, simple echo summation would only add noise from later echo images to the total signal. In contrast, BOLD-signal changes in nondropout regions could already be detected, although not optimally, in echo images with a short TE. Thus, early echo images still contributed by a certain fraction to the total weighted signal in nondropout regions. However, the difference in TNAV between the echo combination schemes was lower than expected. We explain this by relatively small BOLD contrast-to-noise ratio variations over a broad range of TE and the fact that fMRI activity was mainly detected in homogeneous brain regions.

Although the experiments were counterbalanced from one subject to another and from one session to the next (i.e., alternating the order when a particular experiment was performed), variance in BOLD-signal changes due to certain physiologic conditions could not be fully avoided. This issue could be addressed by measuring the BOLD-fMRI signal in every subject several times with unchanged parameters. However, this approach was not suitable for the comparison of different reduction factors as the duration of the whole experiment would have been prohibitively long. As a tradeoff, we repeated the experiment with each volunteer three times in three different sessions and used a breath-hold task, which has the advantage that it does not involve cognitive control. This helped to make the measurements more reproducible and comparable across different settings.

The results from the breath-hold task clearly demonstrated that PERMEATE with $R = 2$ changes and $M = 3$ detected BOLD-signal changes to a larger extent compared to nonaccelerated conventional single-echo EPI. For experiments with $R = 3$, $M = 4$, TNAV was smaller compared to the standard acquisition. We explain this by enhanced *g*-factor noise at 1.5 T for acquisitions with $R = 3$, therefore reducing the benefit of acquiring multiple echoes. Moreover, the total signal readout time for acquisitions with $R = 2$, $M = 3$ is longer compared to acquisitions with $R = 3$, $M = 4$. Therefore, the longer sampling time of the former yields higher SNR, another reason for better results with $R = 2$, $M = 3$.

The benefit of parallel imaging for geometric distortion reduction was somewhat limited. First, compared to diffusion-weighted parallel imaging-accelerated spin echo EPI (2), the acquisition matrix for fMRI scans is typically smaller and hence EPI-induced distortions are much less pronounced; thus, reduced blurring and more accurate signal localization with a resolution of a few millimeters per voxel would not improve the results substantially. Second, adding parallel imaging to single-echo acquisitions lowers SFNR and SNR in a time-normalized fMRI experiment, which in turn reduces the sensitivity of the sequence to BOLD-signal changes. Third, gradient echo EPI suffers from local off-resonance effects as the signal is not refocused by a 180° radiofrequency pulse at TE/2. Thus, image distortions are predominantly due to signal loss that accrued between radiofrequency excitation and TE. Although parallel imaging increased the bandwidth along the phase-encoding direction and thus diminished distortions from chemical shifts, eddy currents, and T_2^* blurring, these artifacts were minimal, especially since for some of them the asymmetric weighting of *k*-space counterbalanced the artifact. Overall, the sacrifice of BOLD sensitivity for small improvements in image resolution and accuracy of spatial localization is unlikely to find application unless a specific demand justifies the use of parallel imaging. Thus, the inclusion of parallel imaging for typical single-echo, single-shot, gradient echo EPI acquired at T_2^* is—at least at 1.5 T—of little advantage for fMRI experiments compared to nonaccelerated single-echo EPI. The true advantage of parallel imaging in concert with gradient echo EPI for fMRI applications derives from the ability to acquire multiple echoes for each time point and thus to acquire images with more optimal BOLD sensitivity.

Caution should be exercised when interpreting these results as scan parameters influence the performance of every sequence. Moreover, the type of array coil and the magnetic field strength at which the experiments were carried out play important roles. As SNR increases with field strength, so also do perturbations from field inhomogeneities and physiological noise. That said, the parallel imaging–induced noise fraction becomes smaller with higher field strength. With increasing amplitude of the static field, another benefit is a more distinct amplitude of the radiofrequency field, allowing one to push parallel imaging to even higher reduction factors without excessive increase in *g*-factor noise, thus facilitating the acquisition of even more echo images without time penalty. Furthermore, higher magnetic field strengths yield stronger image distortions, turning parallel imaging–accelerated multiecho EPI into an even more valuable alternative to single-shot EPI. Initial results at 7 T using the PERMEATE pulse sequence with $R = 4$ were shown by Schmiedeskamp et al. (33), with considerable reduction in signal distortions compared to nonaccelerated acquisitions, maintaining high sensitivity of the pulse sequence to BOLD-signal changes.

CONCLUSION

Despite the ability of parallel imaging to ameliorate image distortions, such as blurring, chemical shift artifacts, or geometric distortions, the major source of image distortions in low-resolution gradient echo EPI comes from T_2^*-related signal decay adjacent to magnetically inhomogeneous areas. This signal loss remains mostly unaffected by parallel

imaging at a magnetic field strength of 1.5 T if TE is unchanged. For parallel imaging–accelerated *single-echo* gradient echo EPI, a significant SNR penalty has to be considered, and hence the overall BOLD-sensitivity is considerably lower compared to nonaccelerated scans. However, using the *multiecho* PERMEATE sequence in concert with parallel imaging, SFNR and therefore temporal signal stability can be improved compared to nonaccelerated conventional single-echo gradient echo EPI, as shown from our fMRI measurements acquired at 1.5 T. Therefore, smaller dropout regions due to image acquisition at shorter TE, slight improvements in image quality by parallel imaging, and an increase in the extent of detected BOLD-signal changes render the use of parallel imaging–accelerated multiecho EPI beneficial over nonaccelerated single-echo EPI for BOLD-fMRI.

Acknowledgments

Support was provided by the Lucas Foundation, Oak Foundation, and August-Karolus-Fund ETH Zurich.

Grant sponsor: National Institutes of Health; Grant numbers: R01EB002711, R01NS047607, R01NS34866, P41RR09784.

REFERENCES

1. Farzaneh F, Riederer SJ, Pelc NJ. Analysis of T2 limitations and off-resonance effects on spatial resolution and artifacts in echo-planar imaging. Magn Reson Med 1990;14:123–139. [PubMed: 2352469]
2. Bammer R, Keeling SL, Augustin M, Pruessmann KP, Wolf R, Stollberger R, Hartung HP, Fazekas F. Improved diffusion-weighted single-shot echo-planar imaging (EPI) in stroke using sensitivity encoding (SENSE). Magn Reson Med 2001;46:548–554. [PubMed: 11550248]
3. Griswold MA, Jakob PM, Chen Q, Goldfarb JW, Manning WJ, Edelman RR, Sodickson DK. Resolution enhancement in single-shot imaging using simultaneous acquisition of spatial harmonics (SMASH). Magn Reson Med 1999;41:1236–1245. [PubMed: 10371457]
4. Pruessmann KP, Weiger M, Scheidegger MB, Boesiger P. SENSE: sensitivity encoding for fast MRI. Magn Reson Med 1999;42:952–962. [PubMed: 10542355]
5. Newbould RD, Skare ST, Jochimsen TH, Alley MT, Moseley ME, Albers GW, Bammer R. Perfusion mapping with multiecho multishot parallel imaging EPI. Magn Reson Med 2007;58:70–81. [PubMed: 17659630]
6. Jochimsen TH, Newbould RD, Skare ST, Clayton DB, Albers GW, Moseley ME, Bammer R. Identifying systematic errors in quantitative dynamic-susceptibility contrast perfusion imaging by high-resolution multi-echo parallel EPI. NMR Biomed 2007;20:429–438. [PubMed: 17044140]
7. Kwong KK, Belliveau JW, Chesler DA, Goldberg IE, Weisskoff RM, Poncelet BP, Kennedy DN, Hoppel BE, Cohen MS, Turner R, Cheng H-M, Brady TJ, Rosen BR. Dynamic magnetic resonance imaging of human brain activity during primary sensory stimulation. Proc Natl Acad Sci U|S|A 1992;89:5675–5679.
8. Ogawa S, Tank DW, Menon R, Ellermann JM, Kim SG, Merkle H, Ugurbil K. Intrinsic signal changes accompanying sensory stimulation: functional brain mapping with magnetic resonance imaging. Proc Natl Acad Sci U|S|A 1992;89:5951–5955.
9. Speck O, Hennig J. Functional imaging by I0- and T2*-parameter mapping using multi-image EPI. Magn Reson Med 1998;40:243–248. [PubMed: 9702706]
10. Posse S, Wiese S, Gembris D, Mathiak K, Kessler C, Grosse-Ruyken ML, Elghahwagi B, Richards T, Dager SR, Kiselev VG. Enhancement of BOLD-contrast sensitivity by single-shot multi-echo functional MR imaging. Magn Reson Med 1999;42:87–97. [PubMed: 10398954]
11. Posse S, Binkofski F, Schneider F, Gembris D, Frings W, Habel U, Salloum JB, Mathiak K, Wiese S, Kiselev V, Graf T, Elghahwagi B, Grosse-Ruyken ML, Eickermann T. A new approach to measure single-event related brain activity using real-time fMRI: feasibility of sensory, motor, and higher cognitive tasks. Hum Brain Mapp 2001;12:25–41. [PubMed: 11198103]

12. Posse S, Kemna LJ, Elghahwagi B, Wiese S, Kiselev VG. Effect of graded hypo- and hypercapnia on fMRI contrast in visual cortex: quantification of T(*)(2) changes by multiecho EPI. Magn Reson Med 2001;46:264–271. [PubMed: 11477629]
13. Posse S, Shen Z, Kiselev V, Kemna LJ. Single-shot T(2)* mapping with 3D compensation of local susceptibility gradients in multiple regions. Neuroimage 2003;18:390–400. [PubMed: 12595192]
14. Weiskopf N, Klose U, Birbaumer N, Mathiak K. Single-shot compensation of image distortions and BOLD contrast optimization using multi-echo EPI for real-time fMRI. Neuroimage 2005;24:1068–1079. [PubMed: 15670684]
15. Poser BA, Versluis MJ, Hoogduin JM, Norris DG. BOLD contrast sensitivity enhancement and artifact reduction with multiecho EPI: parallel-acquired inhomogeneity-desensitized fMRI. Magn Reson Med 2006;55:1227–1235. [PubMed: 16680688]
16. Zysset S, Muller K, Lohmann G, von Cramon DY. Color-word matching Stroop task: separating interference and response conflict. Neuroimage 2001;13:29–36. [PubMed: 11133306]
17. Kruger G, Glover GH. Physiological noise in oxygenation-sensitive magnetic resonance imaging. Magn Reson Med 2001;46:631–637. [PubMed: 11590638]
18. Menon RS, Ogawa S, Tank DW, Ugurbil K. 4 Tesla gradient recalled echo characteristics of photic stimulation-induced signal changes in the human primary visual cortex. Magn Reson Med 1993;30:380–386. [PubMed: 8412612]
19. Kruger G, Kastrup A, Glover GH. Neuroimaging at 1.5 T and 3.0 T: comparison of oxygenation-sensitive magnetic resonance imaging. Magn Reson Med 2001;45:595–604. [PubMed: 11283987]
20. Van de Moortele, PF.; Ugurbil, K.; Lehericy, S. Is T2* always the optimum echo time in BOLD FMRI? Challenging a common concept with a new contrast to noise ratio BOLD model. 16th Annual Meeting of the ISMRM; Toronto, Canada. 2008. p. 2464
21. Griswold MA, Jakob PM, Heidemann RM, Nittka M, Jellus V, Wang J, Kiefer B, Haase A. Generalized autocalibrating partially parallel acquisitions (GRAPPA). Magn Reson Med 2002;47:1202–1210. [PubMed: 12111967]
22. Qu P, Shen GX, Wang C, Wu B, Yuan J. Tailored utilization of acquired k-space points for GRAPPA reconstruction. J Magn Reson 2005;174:60–67. [PubMed: 15809173]
23. Kastrup A, Li TQ, Takahashi A, Glover GH, Moseley ME. Functional magnetic resonance imaging of regional cerebral blood oxygenation changes during breath holding. Stroke 1998;29:2641–2645. [PubMed: 9836778]
24. Thomason ME, Foland LC, Glover GH. Calibration of BOLD fMRI using breath holding reduces group variance during a cognitive task. Hum Brain Mapp 2007;28:59–68. [PubMed: 16671081]
25. Gowland PA, Bowtell R. Theoretical optimization of multi-echo fMRI data acquisition. Phys Med Biol 2007;52:1801–1813. [PubMed: 17374912]
26. Lee AT, Glover GH, Meyer CH. Discrimination of large venous vessels in time-course spiral blood-oxygen-level-dependent magnetic-resonance functional neuroimaging. Magn Reson Med 1995;33:745–754. [PubMed: 7651109]
27. Friston KJ, Jezzard P, Turner R. Analysis of functional MRI time-series. Hum Brain Mapp 1994;1:153–171.
28. Price RR, Axel L, Morgan T, Newman R, Perman W, Schneiders N, Selikson M, Wood M, Thomas SR. Quality assurance methods and phantoms for magnetic resonance imaging: report of AAPM Nuclear Magnetic Resonance Task Group No. 1. Med Phys 1990;17:287–295. [PubMed: 2333055]
29. Reeder SB, Wintersperger BJ, Dietrich O, Lanz T, Greiser A, Reiser MF, Glazer GM, Schoenberg SO. Practical approaches to the evaluation of signal-to-noise ratio performance with parallel imaging: application with cardiac imaging and a 32-channel cardiac coil. Magn Reson Med 2005;54:748–754. [PubMed: 16088885]
30. Glover GH, Lai S. Self-navigated spiral fMRI: interleaved versus single-shot. Magn Reson Med 1998;39:361–368. [PubMed: 9498591]
31. de Zwart JA, van Gelderen P, Kellman P, Duyn JH. Application of sensitivity-encoded echo-planar imaging for blood oxygen level-dependent functional brain imaging. Magn Reson Med 2002;48:1011–1020. [PubMed: 12465111]

32. Wiesinger F, Van de Moortele PF, Adriany G, De Zanche N, Ugurbil K, Pruessmann KP. Potential and feasibility of parallel MRI at high field. NMR Biomed 2006;19:368–378. [PubMed: 16705638]

33. Schmiedeskamp, H.; Newbould, RD.; Bammer, R. Parallel imaging accelerated multi-echo fMRI at 7T. 16th Annual Meeting of the ISMRM; Toronto, Canada. 2008. p. 2368

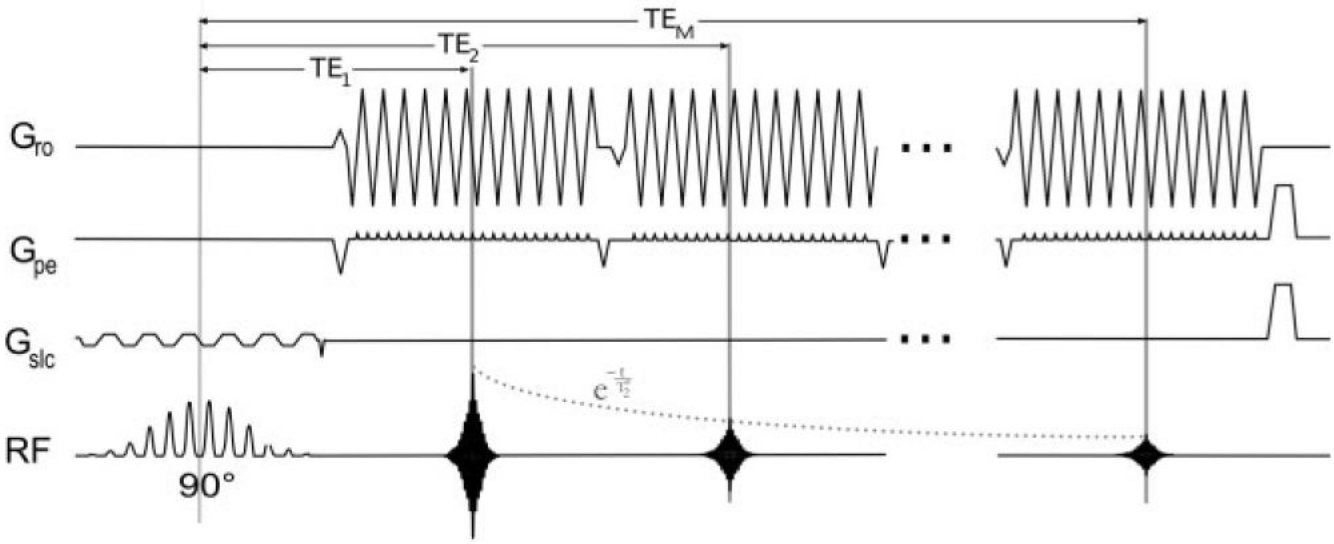

FIG. 1.

PERMEATE pulse sequence design (5) with *M* echo trains (TE ranging from TE_1 to TE_M) following a spectral-spatial excitation pulse. Each echo train represents an *N*-fold undersampled *k*-space, which can be reconstructed into a separate image using GRAPPA weights determined by the first *N* interleaves of each fMRI experiment. G_{ro} = readout gradient, G_{pe} = phase-encoding gradient, G_{slc} = slice-selective gradient, RF = radiofrequency excitation pulse and signal readout.

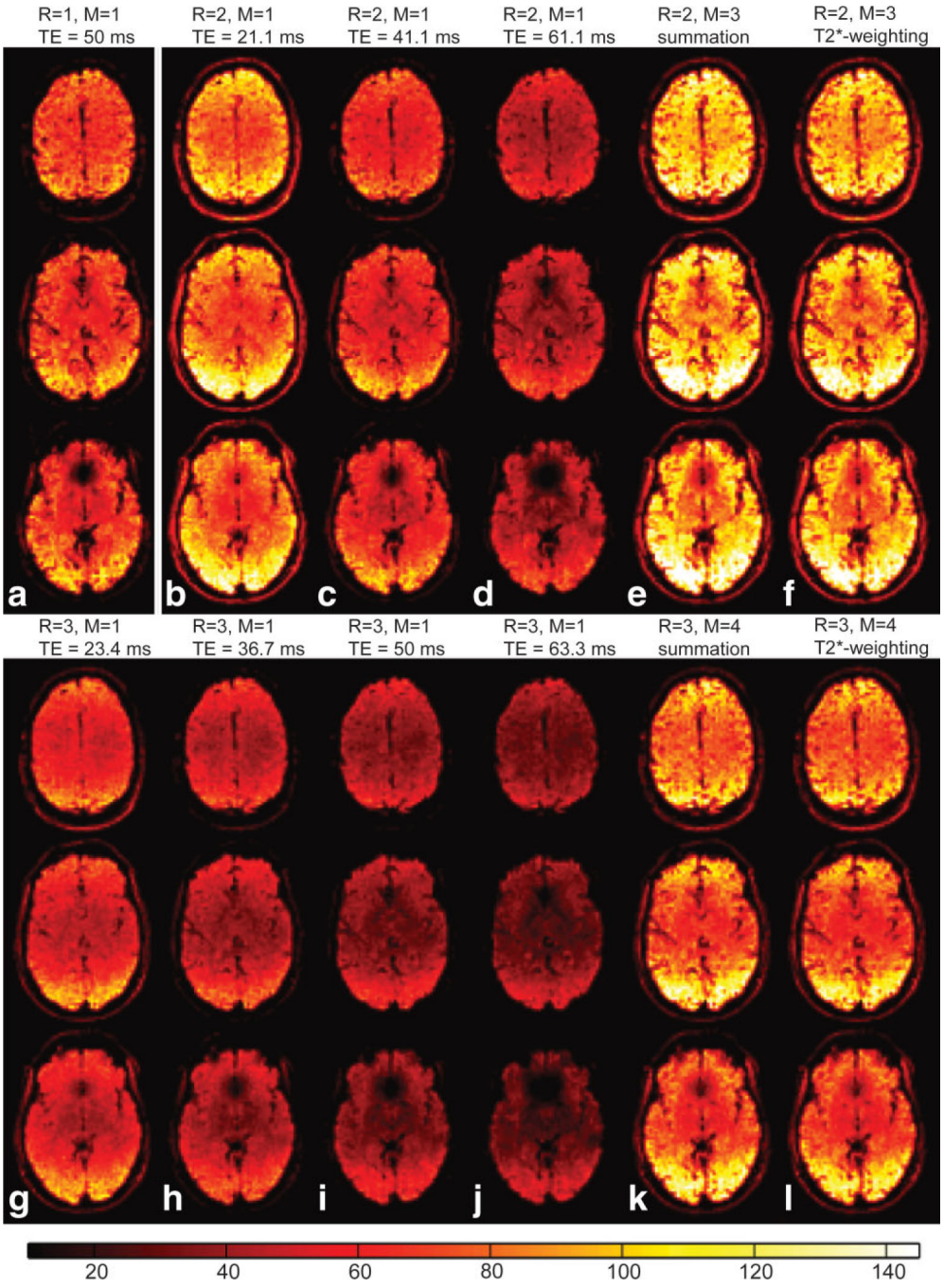

FIG. 2.

SFNR maps of selected slices in subject 1, session #3, for acquisitions with three different reduction factors: (a) $R = 1$, (**b–f**) $R = 2$, and (**g–l**) $R = 3$. For $R = 2$ and $R = 3$, SFNR maps of each individual echo image of a given acquisition are compared to SFNR maps of multiecho images generated using M echoes combined with echo summation (**e,k**) and T_2^*-weighted echo combination (**f,l**). [Color figure can be viewed in the online issue, which is available at www.interscience.wiley.com.]

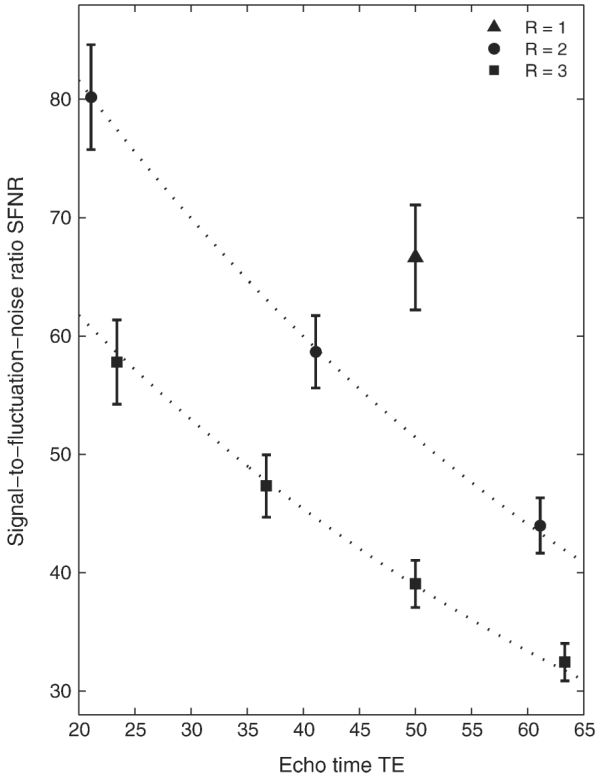

FIG. 3.

Measured SFNR, averaged over all subjects and sessions, retrieved from single-echo analysis ($M = 1$) of acquisitions with reduction factors $R = 1$–3. Dotted lines represent exponential decay of SFNR with $\mathrm{SFNR}(R, \mathrm{TE}) = \mathrm{SFNR}_0(R) \cdot \exp\left(-\mathrm{TE}/T_2^*\right)$, assuming average $T_2^* = 65$ ms. Error bars represent the standard deviations over all subjects and sessions.

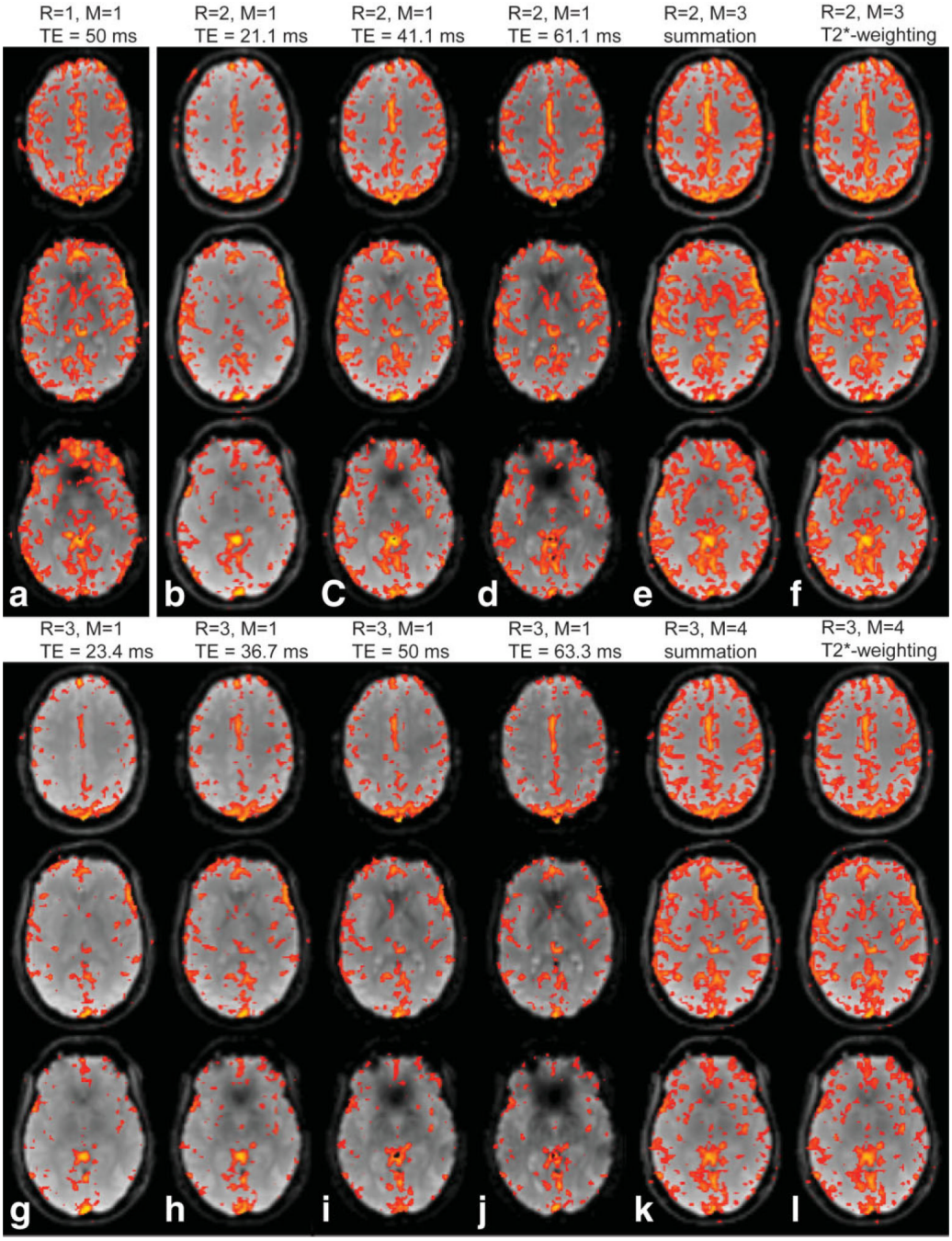

FIG. 4.

fMRI maps of breath-hold experiments for *M*-echo acquisitions with parallel imaging reduction factors $R = 1–3$, shown for each echo image separately ($R = 1$: (**a**), $R = 2$: (**b–d**), $R = 3$: (**g–j**)), as well as for echo summation (**e,k**) and T_2^*-weighted echo combination (**f,l**). Voxels with correlation coefficients $r \geq 0.3$ are highlighted, overlaid onto the average signal of the BOLD-fMRI experiment including only the echo image(s) used for the corresponding analysis.

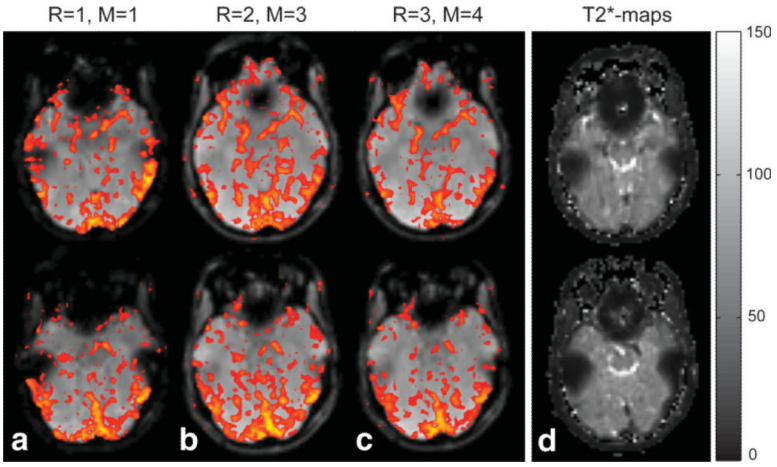

FIG. 5.

Selected slices with dropout regions above nasal cavities and next to the auditory canals, as typically seen in (**a**) nonaccelerated, single-echo, single-shot BOLD-fMRI experiments with long TE = 50 ms ($R = 1$). Using multiecho EPI acquisitions with (**b**) $R = 2$ and (**c**) $R = 3$, BOLD signal changes above threshold could be detected in such dropout regions. **d**: T_2^*-maps of the corresponding slices show particularly small T_2^*-values in these dropout regions (areas of short T^*_2 next to nasal cavities and auditory canals), while larger $T_2^* \approx 50 - 70$ ms was found in more homogeneous brain regions, which do not suffer from the same susceptibility effects.

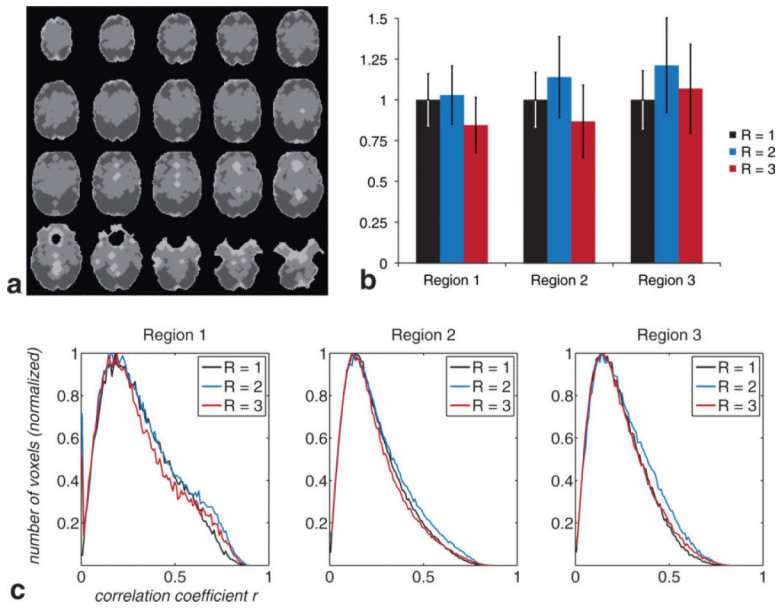

FIG. 6.

Region-specific assessment of multiecho acquisition schemes vs single-echo measurements. Analysis of TNAV and corresponding correlation coefficients separated into three regions (**a**): region 1, containing voxels with low SFNR (light gray); region 2, with average SFNR (medium gray); and region 3, with high SFNR (dark gray). **b**: Region-specific analysis of TNAV for nonaccelerated single-echo acquisition ($R = 1$), 2-fold accelerated three-echo acquisition ($R = 2$), and 3-fold accelerated four-echo acquisition ($R = 3$). Figure indicates average TNAV ± standard deviation over all subjects and sessions, normalized to the acquisition with $R = 1$ for each region. **c**: Histogram showing correlation coefficients for each acquisition scheme (cf. (**b**)), separated into the regions shown in (**a**).

Table 1

TE and EPI Train Length That Were Used in This Study for Different Reduction Factors *R*

Reduction factor	Number of echoes	TE	ETL[a]
$R = 1$	$M = 1$	50.0	37.7 ms
$R = 2$	$M = 3$	21.1, 41.1, 61.1	19.3 ms
$R = 3$	$M = 4$	23.4, 36.7, 50.0, 63.3	12.6 ms

[a]ETL = Echo train length for a single-echo readout.

Table 2

Comparison of Different Acquisition Schemes (Reduction Factor *R*, # of Echoes *M*, Echo Combination Scheme) in Terms of TNAV, SFNR, and SNR

	Acquisition scheme	TNAV	SFNR	SNR
(a)	*R* = 1, *M* = 1, TE = 50 ms	11,594 ± 2182[a] 1.00[b]	66.65 ± 4.43[a] 1.00[b]	57.04 ± 3.69[a] 1.00[b]
(b)	*R* = 2, *M* = 1, TE = 21.1 ms	6486 ± 2555 0.56	80.19 ± 4.43 1.20	63.50 ± 3.78 1.11
(c)	*R* = 2, *M* = 1, TE = 41.1 ms	8844 ± 2773 0.76	58.67 ± 3.06 0.88	48.30 ± 2.59 0.85
(d)	*R* = 2, *M* = 1, TE = 61.1 ms	8769 ± 2624 0.76	43.99 ± 2.33 0.66	37.13 ± 1.85 0.65
(e)	*R* = 2, *M* = 3, Echo summation	13,691 ± 3522 1.18	92.53 ± 6.00 1.39	77.26 ± 6.18 1.35
(f)	*R* = 2, *M* = 3, *T2**-weighted echo combination	13,855 ± 3518 1.19	86.81 ± 5.54 1.30	74.77 ± 4.47 1.31
(g)	*R* = 3, *M* = 1, TE = 23.4 ms	4225 ± 1726 0.36	57.81 ± 3.57 0.87	45.64 ± 2.43 0.80
(h)	*R* = 3, *M* = 1, TE = 36.7 ms	5395 ± 2031 0.47	47.33 ± 2.63 0.71	37.77 ± 1.71 0.66
(i)	*R* = 3, *M* = 1, TE = 50 ms	5636 ± 2122 0.49	39.06 ± 1.99 0.59	31.59 ± 1.37 0.55
(j)	*R* = 3, *M* = 1, TE = 63.3 ms	5393 ± 2071 0.47	32.45 ± 1.58 0.49	26.63 ± 1.04 0.47
(k)	*R* = 3, *M* = 4, Echo summation	10,842 ± 3019 0.94	75.83 ± 6.26 1.14	64.08 ± 4.53 1.12
(l)	*R* = 3, *M* = 4, *T2**-weighted echo combination	10,913 ± 3043 0.94	72.64 ± 5.86 1.09	62.48 ± 3.67 1.10

[a] Average SFNR and SNR ± standard deviation over all subjects and sessions are shown in this table.

[b] Values in the second line of each acquisition scheme are relative to the acquisition with *R* = 1, *M* = 1.